European Neuropsychopharmacology 94 (2025) 24–35

Contents lists available at ScienceDirect

European Neuropsychopharmacology

journal homepage: www.sciencedirect.com/journal/european-neuropsychopharmacology

Chronic mild stress dysregulates autophagy, membrane dynamics, and lysosomal status in frontal cortex and hippocampus of rats

Cristina Ulecia-Morón [a], Álvaro G. Bris [a], Karina S. MacDowell [a], Pilar Cerveró-García [b], José L.M. Madrigal [a], Borja García-Bueno [a], Marta P. Pereira [c], Juan C. Leza [a], Javier R. Caso [a,*]

[a] Departamento de Farmacología y Toxicología, Facultad de Medicina, Universidad Complutense de Madrid (UCM), Centro de Investigación Biomédica en Red de Salud Mental, Instituto de Salud Carlos III (CIBERSAM, ISCIII), Instituto de Investigación Sanitaria Hospital 12 de Octubre (imas12), Instituto Universitario de Investigación Neuroquímica (IUIN, UCM), Madrid, Spain
[b] Departamento de Bioquímica y Biología Molecular, Universidad de Salamanca, Instituto de Neurociencias de Castilla y León (INCyL), Salamanca, Spain
[c] Departamento de Biología Molecular, Universidad Autónoma de Madrid (UAM), Centro de Biología Molecular "Severo Ochoa" (CBMSO, UAM-CSIC), Instituto Universitario de Biología Molecular (IUBM-UAM), Madrid, Spain

ARTICLE INFO

Keywords:
Autophagy
Chronic mild stress
ESCRT
Lysosome
SQSTM1/p62

ABSTRACT

Inflammation has been related to major depressive disorder pathophysiology. Autophagy, a degradative pathway regulating inflammation and immunity, has emerged as a potential contributor. Among others, we characterized, in frontal cortex (FC) and hippocampus (Hp), autophagy markers (upregulations in mTOR, ATG7, and ATG 16L1, and downregulations in ULK1, BECLIN1, phospho-SQSTM1, ATG3, ATG12, and ATG 16L1), effectors of the endosomal sorting complexes required for transport (overexpression in HRS, VPS37A, CHMP6, and GALECTIN 3, and downregulations in STAM2, TSG101, VPS28, VPS37A, CHMP5, VPS4B, and GALECTIN 9), and lysosomal proteins (LAMP1, LAMP2A, MANNOSE RECEPTOR, HSC70, HSP70, CATHEPSIN D and B, and CYSTATIN C, whose variations are dependent on lysosomal nature and brain region) of male rats exposed to chronic mild stress, a model of depression, compared to control rats. Results indicate that chronic stress alters protein expression of autophagy and the endosomal sorting complexes required for transport markers in a region-specific manner, plus increases lysosomal presence, oppositely modulating lysosomal proteins in each structure. Additionally, astrocytes seemed to exert an essential role in the regulation of the autophagy adaptor SQSTM1/p62. In conclusion, stress-induced protein disruptions in these pathways highlight their differential modulation after chronic stress exposure and their potential role in maintaining brain homeostasis during the stress response, making them promising targets for new therapeutic strategies in stress-related pathologies.

1. Introduction

Major depressive disorder (MDD) is one of the leading causes of disability, playing a significant part in the overall global burden of disease (Beurel et al., 2020; Collaborators GBDMD, 2022). Although the pathophysiology of MDD is not entirely understood, it is hypothesized that multiple factors contribute to its onset, with chronic stress exposure being one of the main triggers (Arango et al., 2021; Yang et al., 2015).

Stress persistence can generate an imbalance between the production of reactive oxygen and nitrogen species and the endogenous antioxidant system of the cell (Bhatt et al., 2020), the accumulation of which is extremely detrimental to brain cells when in excess (Madrigal et al., 2001), and can lead to inflammation (Madrigal et al., 2002). Clinical studies have demonstrated that MDD patients present a chronically systemic inflammatory status (Troubat et al., 2021), together with systemic immune activation (Pandey et al., 2019).

Autophagy is a lysosome-dependent recycling system responsible for the degradation of protein aggregates, dysfunctional organelles, and bacteria. Through this process, the material destined for elimination is enclosed within a double-membrane structure known as an autophagosome, which subsequently fuses with lysosomes, facilitating the digestion and recycling of its key components (Deretic, 2021).

* Corresponding author at: Department of Pharmacology and Toxicology, School of Medicine, Universidad Complutense de Madrid, Plaza Ramon y Cajal s/n, 28040, Madrid, Spain.
E-mail address: jrcaso@med.ucm.es (J.R. Caso).

https://doi.org/10.1016/j.euroneuro.2025.02.005
Received 19 July 2024; Received in revised form 7 February 2025; Accepted 11 February 2025
Available online 7 March 2025

Autophagy is a homeostatic mechanism closely linked to the inflammatory response and plays a crucial role in the central nervous system, contributing to neuronal viability, synapse formation and remodeling, axonal development, and spine pruning, among other functions (Deretic, 2021; Gassen and Rein, 2019).

Studies have associated defective autophagy with the development of neuropsychiatric diseases (Tomoda et al., 2020): postmortem samples of MDD subjects have shown defective mTOR signaling in the frontal cortex (FC) (Jernigan et al., 2011); a positive correlation was found between BECLIN1 protein levels in peripheral blood mononuclear cells (PBMC) and treatment response (Gassen et al., 2014); additionally, it was observed that neuronal autophagy pathways were vital in MDD and modulated antidepressant effects (Jia and Le, 2015). In animal studies, antidepressants were found accumulated within lysosomes, suggesting lysosome-dependent degradation (Gulbins et al., 2018). Furthermore, mice exposed to stress had lower levels of BECLIN1, microtubule-associated protein 1A/1B-light chain 3 (LC3), and sequestosome-1 (SQSTM1/p62) in the hippocampus (Hp) (Xiao et al., 2018).

The endosomal sorting complex required for transport (ESCRT) machinery has recently emerged as a crucial component of several subcellular processes (Remec Pavlin and Hurley, 2020). Concretely, ESCRT complex dysfunction contributes to autophagosome accumulation in mammals (Habib et al., 2021), and participates in lysosomal and plasma membrane repair, nuclear pore structure, and neuronal pruning (Vietri et al., 2020). To our knowledge, no characterizations of the ESCRT complex have been conducted in either animal models or human samples of neuropsychiatric pathologies so far.

Since FC and Hp are brain regions that mediate aspects of MDD (Nestler et al., 2002), we investigated the effects of chronic mild stress (CMS) on both regions in rats, digging deeper into different levels within the autophagy molecular pathway, beyond its chief markers. To achieve this, we evaluated protein and RNA expression levels of autophagy markers and representative protein concentrations of each subcomplex within the ESCRT machinery. Additionally, lysosomal homeostasis was examined via lysosome separation into light and heavy lysosomes, each obtained fraction dedicated to the study of proteases and proteins involved in the chaperone-mediated autophagy (CMA), a specific subtype of autophagy. Colocalization analyses were also performed to elucidate the role of neurons, astrocytes, and microglia in some of the protein modifications observed after CMS (see **Supplemental Figure S1** for Graphical depiction of the autophagy pathway).

2. Experimental procedures

2.1. Animals

Male Wistar Hannover rats (HsdRccHan:Wist, ENVIGO, Spain) weighing 200–225 g were individually caged and kept under temperature and humidity standard conditions, and at a 12 h light/dark cycle (8:00 a.m.−8:00 p.m.). Rats had access to food and water *ad libitum* during 14 days prior to the beginning of the stress protocol. All experimental approaches followed the guidelines of the Animal Welfare Committee of the Complutense University (PROEX/098/19) and Madrid Regional Government according to European legislation (2010/63/EU). Animal studies are reported in compliance with the ARRIVE guidelines. All efforts were focused on minimizing the suffering and reducing the number of animals employed.

Rats were randomly divided into two experimental groups: Control group (CT) and CMS group, whose *n* vary according to each biochemical determination and will be specified accordingly. See **Supplemental Figure S2** for Visual representation of the experimental design of the study.

2.2. CMS protocol

The protocol is a modification of the one described by Willner (2005). Our group has previously demonstrated how this protocol induces a depressive-like behavior in Wistar male rats, evaluated through several behavioral tests (i.e., sucrose test, forced swim test, splash test, and elevated plus maze test (Bravo et al., 2012)). For 21 days, rats were exposed to two stressors per day, these changing every 12 h. The stressors included: soiled caged, food/ water deprivation, cage tilting, paired housing, stroboscopic illumination, and intermittent illumination.

2.3. Autophagy flux assay

Vehicle (veh) and leupeptin (leu) groups (7–9 rats per group) were anesthetized with isoflurane (ELASA, Spain). When there was no response at physical stimulation (paws, tail, and vibrissa) stereotaxic surgery was performed. Heads were then placed in the frame of the stereotaxic device (Stoelting, USA), and after the skulls were exposed, they were drilled with a 23 gauge needle with a 0.635 mm outer diameter. This opening allowed the insertion of a 22 gauge needle (Hamilton Company; 22 gauge, Small Hub RN NDL, length 0.75 in, point style 4 cut at an angle of 10–12°) held in the attached syringe (Hamilton Company; 10 μl, Model 701 RN, 26 s gauge, 51 mm, point style 2) and lowered into the brain to inject 10 μl of 20 mg/kg of leu or saline at the speed of 1 μl/min in the FC (coordinates from Bregma: 4.2 mm A/P, 1.5 mm M/L, 1.8 D/V) and in the Hp (coordinates from Bregma: −3.6 mm A/P, 2 mm M/L, 3 mm D/V). Both injections were carried out on both hemispheres. Once the injection was completed, the needle was removed from the incision after 2 mins. The skull incision was sealed with bone wax (Surgical Specialties Corp, 901), and the wound was sutured with non-absorbable silk (B. Braun, Germany). Three hours post-injection, the FC and Hp of vehicle-treated and leupeptin-treated rats were collected as described in the Supplementary Experimental Procedures. The LC3II:LC3I protein ratio was analyzed via Western blot (WB) in each brain region from the same animals.

2.4. Sample collection

To avoid any variation among groups due to circadian rhythms, samples were always obtained between 1:00 p.m. and 3:00 p.m. Control group samples were collected one or two days after those from the CMS group. Collection and processing are detailed in the Supplementary Experimental procedures. Blood samples were obtained through cardiac puncture and anti-coagulated with Ethylenediaminetetraacetic acid (EDTA, Sigma-Aldrich, 15 % w/v, 1 vol EDTA per 9 vol blood).

2.5. Tissue homogenization and immunoblotting

Pure cytosolic fractions were isolated without nuclear contamination by employing a widely used protocol (Schreiber et al., 1989). Briefly, FC and Hp were homogenized in 600 μl and 400 μl respectively of buffer (10 mmol/l N-2-hydroxyethylpiperazine-N-2-ethanesulfonic acid [pH 7.9], 1 mmol/l EDTA, 1 mmol/l EGTA, 10 mmol/l KCl, 1 mmol/l dithiothreitol, 0.5 mmol/l phenylmethylsulfonyl fluoride, 0.1 mg/ml aprotinin, 1 mg/ml leupeptin, 1 mg/ml Na-p-tosyll-lysine-chloromethylketone, 5 mmol/l NaF, 1 mmol/l NaVO4, 0.5 mol/l sucrose, and 10-mmol/l Na2MoO4). After 15 min, Nonidet P-40® (Sigma-Aldrich, 74,385) was added to reach a 0.5 % concentration. Tubes were vigorously vortexed for 15 s twice, and nuclei were pelleted by centrifugation at 8000 x *g* for 5 min. Supernatants were considered as the cytosolic fractions. Every step was performed at 4 °C.

To determine protein expression levels of different markers in FC and Hp, the Bradford assay was carried out. Once protein levels were adjusted and mixed with Laemmli sample buffer (Bio-Rad, 1610737) and β-mercaptoethanol (20:1; AppliChem A4338), 15 μg (20 μg for CHMP5, CHMP6, and LC3II:LC3I ratio) of protein were loaded into SDS-polyacrylamide gels to perform electrophoresis (100 V). When completed, gels were transferred onto 0.2 μm nitrocellulose membranes

(PDVF for the LC3 protein blotting) (Bio-Rad, 1704159 and 1704157) using a semi-dry transfer system (Bio-Rad, USA). Membranes were blocked in Tris-buffered saline 1x (TBS 10x: 200 mM Tris, 1500 mM NaCl, pH 7.6) supplemented with 0.1 % Tween 20 (BioRad, 1706531) and 5 % Bovine Serum Albumin (BSA; AppliChem, A6588), for later to be incubated with specific primary antibodies overnight at 4 °C (**Supplemental Table S1**). After washing with TBS containing 0.1 % Tween 20 (TBSt), membranes were incubated with secondary antibodies conjugated to horseradish peroxidase (HRP) for 1 h 30 min at room temperature and revealed with ECL® kit following manufacturer's instructions (Fisher Scientific, 12,994,780) using the Odyssey® Fc System (Li-COR Biosciences, USA). To ensure the linearity of the band intensities, correct protein transfer through Ponceau staining was verified prior membrane transference, different exposition times were considered, and signal saturation was avoided. Also, preliminary serial dilutions of control samples were initially run to ensure band intensities correlated linearly with the protein amount. Several conditions were set to guarantee the selection of the chosen bands (i.e., antibodies titration, incubation times, negative controls). The loading housekeeping control was β-ACTIN (Sigma-Aldrich, A5441). Bands were quantified by densitometry by means of the NIH ImageJ® software. Results are expressed as percentage compared to CT group, after being normalized by β-ACTIN levels. All these WB were repeated at least five times for each protein in separate assays, to ensure the reproducibility of the results. The number of animals used was CT ($n = 7$) and CMS ($n = 14$) in FC, and CT ($n = 7$) and CMS ($n = 10$) in Hp. Since Hp is a smaller area than FC, fewer animals were studied to employ the remaining hippocampi in other determinations.

2.6. RNA extraction and RT-QPCR analyses

TRIzol® reagent (Invitrogen, USA) was used to extract total RNA from FC and Hp, and then homogenized in the TissueLyser LT (Quiagen, Netherlands). Aliquots of each sample were converted into cDNA using random hexamer primers (Invitrogen, USA). Quantitative changes in mRNA levels were detected by real-time (RT) quantitative polymerase chain reaction (RT-qPCR) with the following conditions: 35–40 cycles of denaturation at 95 °C (10 s), annealing at 63 °C (15 s), and extension at 72 °C (20 s). Reactions were performed in the presence of SYBR Green (Biotools, 10,606–4153) in a Corbett Rotor-Gene (Corbett Research, Australia) in 20 µl. Relative mRNA concentrations were calculated from the take-off point of reactions. To normalize the data, tubulin expression was used as the housekeeping gene. Primer3 tool (Untergasser et al., 2012) was used to design specific primers (**Supplemental Table S2**). To verify target specificity, an in-silico PCR simulation (USCS Genome-Browser) and Blast (NCBI) were run. Triplicate measurements of each aliquot were assayed, together with a negative internal control in each run. The same number of animals as in the previous section was employed.

2.7. Immunofluorescence (IF)

Brain slices were washed several times with 0.012 M potassium phosphate buffer (KPBS) buffer (3.3 mM KH_2PO_4, 8.7 mM $K_2HPO_4{\cdot}3H_2O$, pH 7.4) and incubated with 100 mM glycine (AppliChem, A1067) to reduce autofluorescence. After another set of washes, brain sections were blocked in KPBS supplemented with 10 % BSA and 0.3 % Triton X-100 (Sigma-Aldrich, T8787) for 1 h at room temperature. Then, primary antibodies were diluted in the same buffer and incubated 48–72 h in agitation at 4 °C (**Supplemental Table S3**). Subsequently, brain sections were rinsed and incubated with secondary antibodies for 1 h 30 min at room temperature. After another wash with KPBS, they were incubated with 4′,6-diamidino-2-phenylindole dihydrochloride (DAPI; Sigma-Aldrich, MBD0015) for 4 min at room temperature. Slices were washed again and mounted on slides with Fluoroshield® (Sigma-Aldrich, F6182) and coverslipped. Immunostainings were stored at 4 °C until visualized. Confocal images were obtained using a Leica SP8 confocal microscope, at the CAI-UCM *Centro de Citometría y Microscopía de Fluorescencia.*

NIH ImageJ® software was utilized for quantification analyses. Intensity mean of fluorescence, number of pixels, and number of cells were evaluated (the latter, using the cell counter plugin software), taking into consideration the double immunostaining in each case, from images taken at 20 X. For colocalization studies (p-SQSTM1 vs GFAP), JACoP plugin was employed to obtain Pearson's, Manders', and the Overlapping Coefficients, also from images taken at 20 X. Intensity means are expressed as arbitrary units (A. U.). For triple immunostaining (LAMP2A, MAP2, and IBA1), analyses were carried out through double immunostainings (LAMP2A vs MAP2 and LAMP2A vs IBA1) to ensure less artifacts could interfere in the analysis. Only one set of samples were analyzed at 63 X: LAMP2A vs IBA1, where intensity mean, number of cells, and the percentage of the occupied area were calculated. 20 X images are shown with a 200 µm scale bar, whereas 63 X ones correspond to 30 µm. Brain slices from Bregma +3.7 mm (FC) and Bregma −3.80 mm (Hp) were examined.

2.8. Lysosomal isolation and biochemical determinations

Lysosomal purification was accomplished with a Lysosome Isolation kit (LYSISO1, Sigma-Aldrich) from fresh brain samples following manufacturer's instructions. Both Crude Lysosomal Fraction (CLF) and purified lysosomal fractions were tested for acid phosphatase levels and lysosomal integrity using an Acid Phosphatase Assay kit (MAK446, Sigma-Aldrich) following the manufacturer's guidelines and read at 405 nm. In the same way, Neutral Red reagent (included in the Lysosomal Isolation Kit) was exposed to lysosomal fractions and measured during 5 min, making one read every minute at both 460 and 510 nm. All these reads were made by the microplate reader Synergy 2 (BioTek Instruments, Germany).

2.9. Corticosterone assay

Corticosterone levels were measured using a commercially available ELISA kit (Enzo-LifeSciences, USA).

2.10. Statistical analyses

Data are expressed as mean ± SEM in both text and figures. Outliers were identified using the ROUT method. To examine Gaussian distribution, the Shapiro-Wilk normality test was applied. When the sample distribution was normal, a two-tailed unpaired Student's *t*-test was applied, comparing CT vs CMS (FC and Hp individually considered). If the standard deviation was not equal between CT and CMS, Welch's *t*-test was applied. When distribution was not Gaussian, Mann-Whitney test was performed. Statistical data in terms of F, t, df (Student's *t*-test), U and ranks (Mann-Whitney test), and *p* values are detailed in **Table S6 and Table S8**. For multiple comparisons, a two-way analysis of variance (ANOVA) was used to compare all pairs of means among groups, followed by the Tukey *post-hoc* test. CMS and leupeptin injection, as well as their interaction, were the two factors compared and these analyses are displayed in **Table S7**. A $p < 0.05$ was considered statistically significant.

3. Results

3.1. CMS alters autophagy protein markers both in FC and HP, and ATG genes in HP

There are four main steps within the autophay process: initation, nucleation-elongation, autophagosome fusion with the lysosome, and degradation. Representative markers of each step (see **Suplemental Figure S1**) were selected to be analyzed at the RNA and protein levels.

CMS caused the reduction of phospho(p)-unc-51-like kinase 1 (ULK1), ULK1, BECLIN1, p-SQSTM1, ATG3, and ATG 16L1 protein expression in FC (red bars) compared to control, whereas p-mTOR, BECLIN1, p-SQSTM1, ATG3, and ATG12 expression levels were lower in Hp (blue bars). Only mTOR and ATG7 in FC, and ATG 16L1 in Hp were found to be increased (Fig. 1**A** and **Table S6**). LC3, whose isoform LC3II indicates autophagosome maturation, was studied through the inhibitor leupeptin (leu), allowing the autophagic flux examination. LC3II levels tended to increase in CMS+leu group in FC, despite no interaction between CMS and leupeptin injection was observed in FC. The LC3II:LC3I ratio decreased in the CMS group in Hp in comparison to both CT + vehicle (veh) and CT + leu groups, while CMS + leu showed higher levels compared to CMS + veh. No interaction was observed in Hp (Fig. 1**B** and **Table S7**).

Apoptotic markers were also assayed (not shown, **Figure S3**) and found to be distinctly regulated after CMS exposure. Regarding gene expression, the induction of *Atg7* was observed in FC, whereas *Atg3, Atg5, Atg7*, and *Atg12* were upregulated in Hp (Fig. 1**C** and **Table S6**). Genes that did not undergo any variation are displayed in **Supplemental Figure S4**.

The CMS + leu group showed three times more corticosterone in plasma than any other group (Fig. 1**D** and **Table S7**).

3.2. Phosphorylation of SQSTM1/p62 colocalizes with cortical and hippocampal astrocytes, and CMS increases their hippocampal colocalization

Given the similar results observed in p-SQSTM1 in both regions, the autophagy-related phosphorylation in Ser403 of SQSTM1/p62 protein was assayed by immunofluorescence and compared to the astrocyte marker glial fibrillary acidic protein (GFAP) in some areas of the FC and Hp (Fig. 2). This posttranslational modification was widely observed throughout the astrocytic body in FC and Hp, regardless of CMS exposure. CMS promoted a higher colocalization ratio in some areas of the FC and Hp, especially in astroglial ramifications (Fig. 2**A**). CMS resulted in an enhanced colocalization rate of p-SQSTM1-GFAP in the secondary motor cortex (FC) and the dentate gyrus (DG), hilar cells of the DG, and CA3 (Hp), as demonstrated in terms of Pearson's Coefficient, Overlap Coefficient, and Manders' Coefficient (Fig. 2**B).**

3.3. Cortical and hippocampal ESCRT machinery is affected by the CMS

The ESCRT complex is involved in phagophore sealing and autophagosome formation. Hepatocyte growth factor-regulated tyrosine kinase substrate (HRS) and signal transducing adaptor molecule 2 (STAM2) (components of the ESCRT-0 complex) were oppositely modified in the FC by CMS, with HRS protein levels increasing and STAM2 levels decreasing; tumor susceptibility gene 101 (TSG101), vacuolar protein sorting-associated protein 28 (VPS28), and 37A (VPS37A) (components of the ESCRT-I complex) were downregulated in FC, while in Hp, TSG101 also decreased, but VPS37A was increased; vacuolar protein sorting-associated protein (VPS25) (components of the ESCRT-II complex) did not show any difference between CT and CMS; charged multivesicular body protein 5 (CHMP5) and charged multivesicular body protein 6 (CHMP6) (components of the ESCRT-III complex) did not exhibit any change in Hp, but increased and decreased, respectively, in FC. As an ESCRT-associated protein, vacuolar protein sorting-associated protein 4B (VPS4B) was assayed and showed a reduction of its levels in Hp (Fig. 3**A** and **Table S6**). Neither RAB5 nor RAB7 showed changes, whereas lower GALECTIN9 (GAL9) levels were observed in both regions. GALECTIN3 (GAL3) was conversely augmented in FC exclusively (Fig. 3**B** and **Table S6**).

3.4. CMS boosts lysosomal acid phosphatase concentrations in CLF and purified fractions in FC and HP

The lysosomal marker acid phosphatase was examined in Crude Lysosomal Fractions (CLF) and six purified fractions (named Lyso 1 to Lyso 6) (Fig. 4**A**): its higher concentrations after CMS were greater in FC than Hp, being consistent among all fractions.

3.5. Light and heavy lysosomes exert differential protein expression changes caused by the CMS

Determinations of protein expression levels of chaperone-mediated autophagy (CMA) and lysosomal-related proteins were performed by WB. Since the lysosome isolation kit enabled the separation of different lysosomal populations (light vs. heavy) into specific fractions, all markers were analyzed across these fractions. In the CLF, composed of all kinds of lysosomes, lysosomal-associated membrane protein 1 (LAMP1) and lysosomal-associated membrane protein 2A (LAMP2A) increased considerably in FC, while the former showed the same increase in Hp but LAMP2A decreased following CMS (Fig. 4**B**). In all the fractions except for Lyso 2 (FC and Hp), LAMP2A was reduced compared to CT. LAMP1 bands could not be detected from Lyso 3 to Lyso 6. Heat shock cognate 70 (HSC70), a crucial player together with LAMP2A in the CMA, showed lower levels in FC but higher in Hp in the CLF, contrary to the LAMP2A protein profile. In Lyso 1, 3, and 4, HSC70 values increased compared to CT in Hp, whereas it was found to be downregulated in the rest of the conditions and fractions. Heat shock protein 70 (HSP70) displayed a very similar pattern, only differing in its elevation in FC in Lyso 3 and the reduction of its levels in both FC and Hp in Lyso 1.

Regarding lysosomal functionality, mature CATHEPSIN D could not be detected in Lyso 3 and Lyso 6 but increased greatly in Lyso 2 in both areas, while its presence dropped in CLF in FC and Hp compared to CT. Proenzyme CATHEPSIN B was reduced in FC of CLF and lysosomal fractions, except for Lyso 1 (where no changes were observed) and Lyso 3 (where no bands were detected). In Hp, it was augmented in CLF, Lyso 4, and Lyso 6. Active CATHEPSIN B showed similar modification trends, except for CLF and Lyso 2, whose hippocampal values were upregulated compared to CT, although the proenzyme did not change in Lyso 2. This form was also detected in Lyso 3, where lower protein values were observed in Hp compared to CT groups.

Lastly, CYSTATIN C was increased in Lyso 1 and 2 in both brain structures, and in hippocampal Lyso 3. In CLF, only Hp showed a protein rise. There were reductions in FC Lyso 4 and hippocampal Lyso 5 (cortical Lyso 5 was increased). Finally, no bands were detected in Lyso 6 (Fig. 4**B**).

To evaluate lysosomal integrity, Neutral Red Uptake was also analyzed in the purified fractions. CMS presented a different uptake rate in FC and Hp, but not sufficiently significant to affirm CMS can modify lysosomal integrity. Lyso 6 was the most sensitive fraction to CMS (Fig. 4**C**).

3.6. CMS induces LAMP2A expression in cortical neurons and microglia, while reduces LAMP2A presence in hippocampal CA1 neurons

Being LAMP2A key for the CMA, triple immunostainings of LAMP2A, microtubule-associated protein 2 (MAP2) (a neuronal marker), and ionized calcium-binding adapter molecule 1 (IBA1) (a microglial marker) were performed in FC and Hp (Fig. 5). The three proteins showed an increase in comparison to their respective controls in the primary motor cortex (and also in the secondary motor cortex, although no LAMP2A changes were observed in the agranular insular cortex and the medial-ventral orbital cortex; **Supplemental Figure S5A**). After CMS, the amount of LAMP2A expressed exclusively by the microglia occupied less space, while enlarged microglial somas and ramifications were observed (Fig. 5**A**). In the Hp, the CMS group showed in CA1 (and in the molecular layer of the DG; **Supplemental Figure S5B**) a

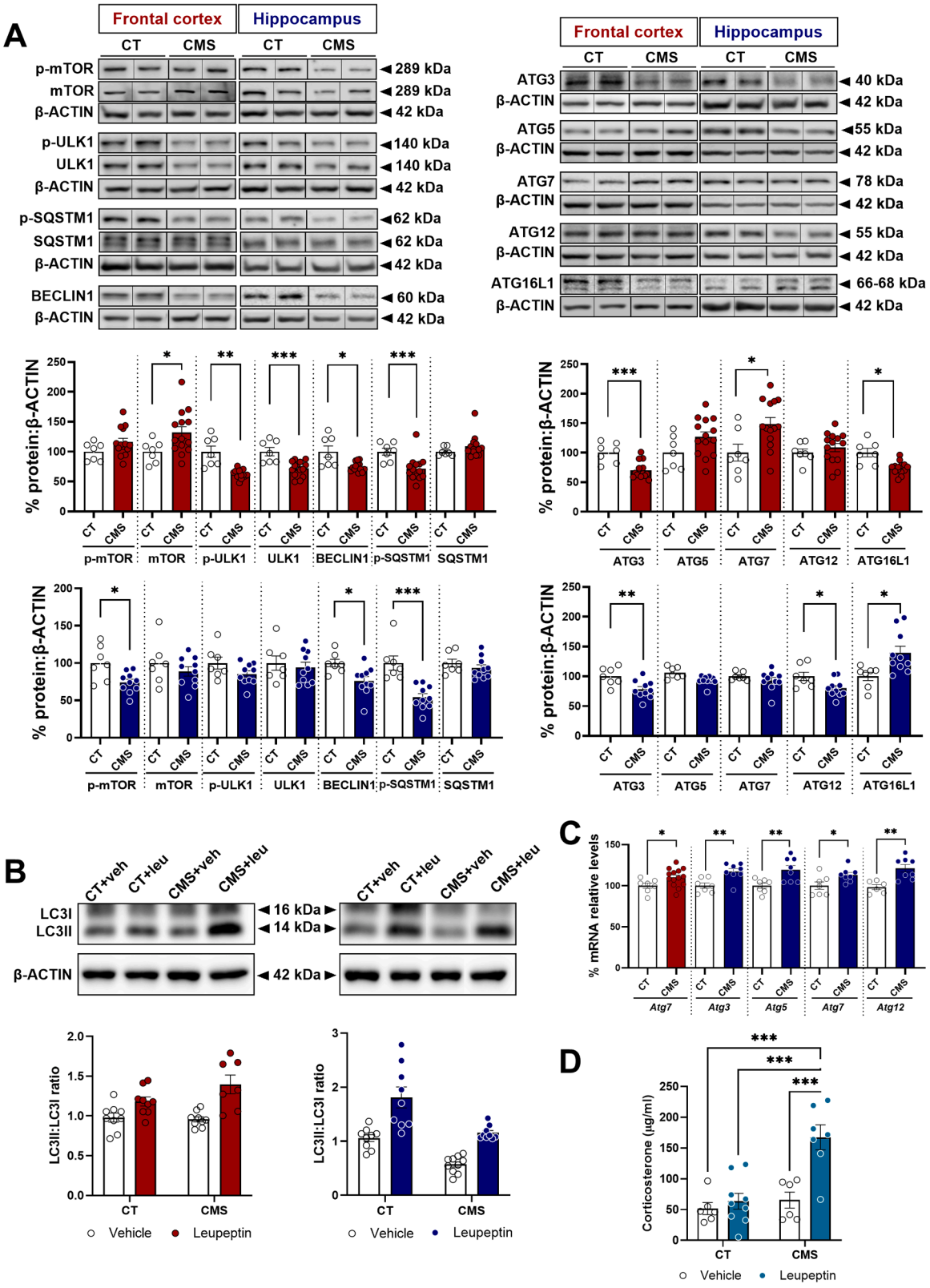

Fig. 1. Autophagy markers are altered at protein and mRNA levels due to the CMS. CMS distinctively shifted autophagy proteins evaluated by WB (**A**). Total inhibition of the autophagic flux was not reached, but a difference between FC and Hp was observed (**B**). *Atg3, Atg5, Atg7,* and *Atg12* presented a different expression after CMS exposure compared to CT (**C**). Genes with no change detected by RT-qPCR are shown in **Figure S4.** As CMS is a stress-based model, corticosterone levels were evaluated by ELISA (**D**). Every marker is expressed as the comparison between the CMS and the CT group in percentage. Two-tailed Student *t*-test was applied in the analysis of each marker (**A** and **C**), whereas a two-way ANOVA was employed to study the LC3II:LC3I ratio and corticosterone levels (**B** and **D**). Data is expressed as mean ± SEM of 7–9 CT and 9–14 CMS rats. ($*p < 0.05$;$**p < 0.01$;$***p < 0.001$;$****p < 0.0001$).

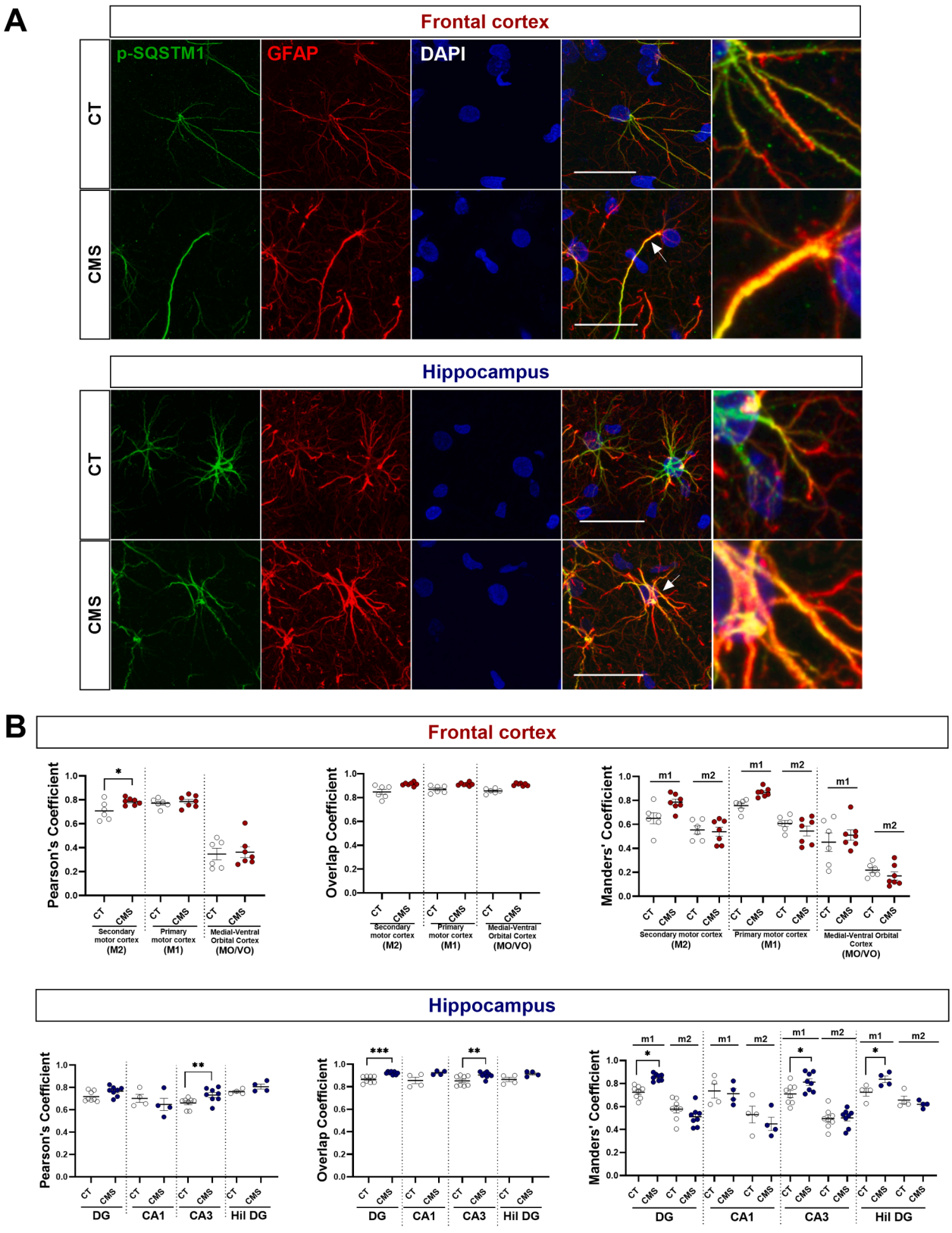

Fig. 2. Colocalization of p-SQSTM1 and GFAP expression in FC and Hp. Brain sections were incubated with p-SQSTM1 and GFAP simultaneously and imaged with a magnification of 20 X (to quantify fluorescence intensities, not shown) and 63 X (**A**) in FC and Hp. Colocalization analyses were performed through the Pearson's Coefficient, Overlap Coefficient, and Mander's Coefficient. FC had a high level of p-SQSTM1 and GFAP overlapping in three areas of the FC, but only the secondary motor cortex had a higher Pearson's Coefficient in the CMS group (**B**). In Hp, CMS improved said colocalization in CA3, DG, and hilar cells, as they expressed a higher Pearson's, Manders', and Overlapping Coefficients when compared to their CT (**B**). An example of this enhanced colocalization is visualized in hippocampal CA3 cells exhibited in **A**. Scale bars stand for 30 μm. Two-tailed Student *t*-test was used in the analysis of each marker. Data is expressed as mean ± SEM 6–8 CT and CMS rats. (*$p < 0.05$;**$p < 0.01$).

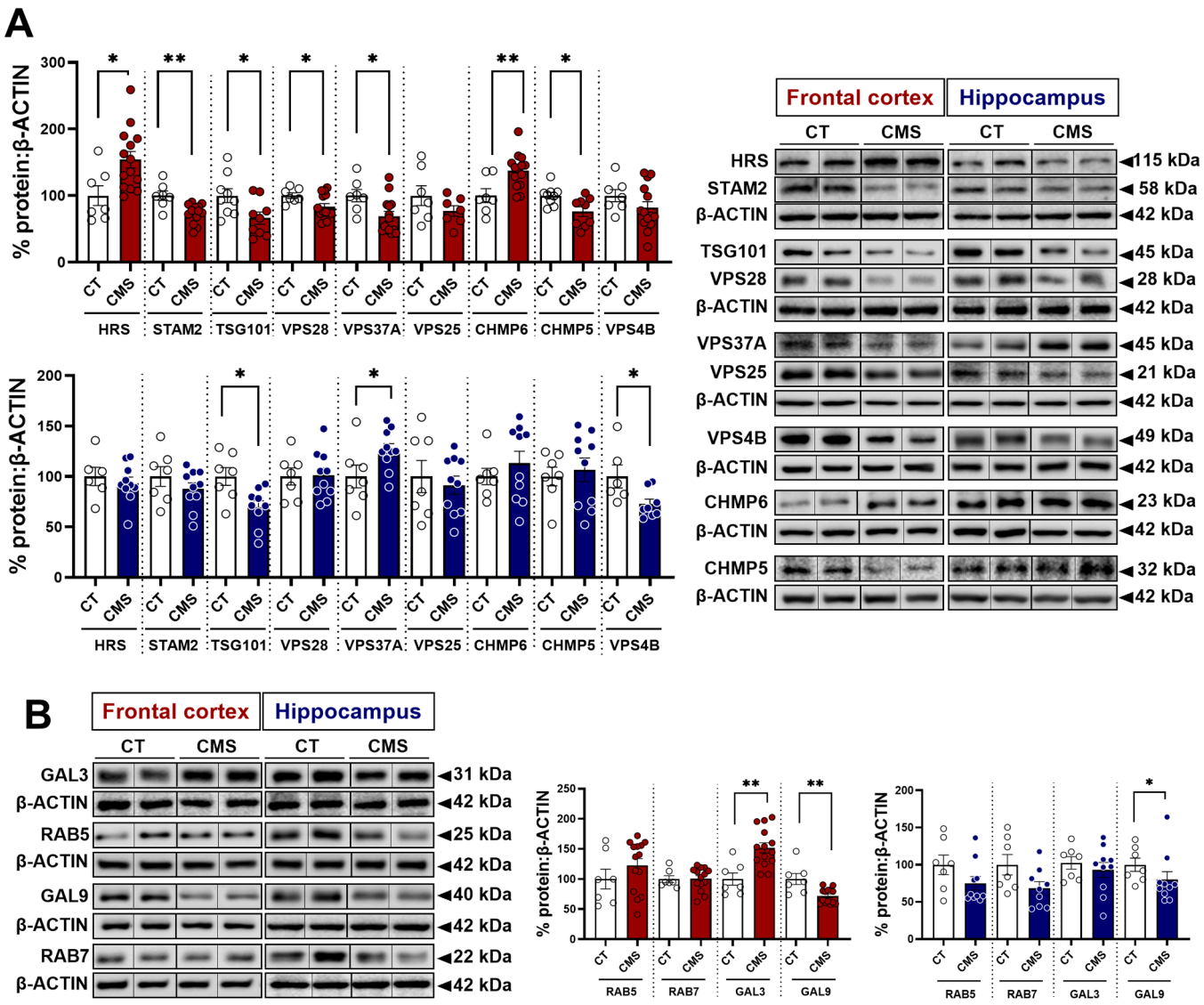

Fig. 3. Protein expression levels determination of some components of the ESCRT machinery. Complexes ESCRT-0, -I, -II, and -III were analyzed through their most common proteins in CMS groups and compared to CT in each brain structure. Almost every protein was altered in FC due to chronic stress, where VPS25 and VPS4B were the ones with no modification. Hp experienced protein changes in TSG101, VPS4B, and VPS37A: the two formers presented a downregulation, while the latter the opposite (**A**). Other proteins that normally assist on the regular ESCRT machinery function were also tested: GALECTIN9 (GAL9) was reduced in both regions and GALECTIN3 (GAL3) increased in FC. RAB5 and RAB7 were unaltered by the CMS (**B**). Two-tailed Student *t*-test was used in the analysis of each marker. Data is expressed as mean ± SEM of 7–9 CT and 9–14 CMS rats. ($^{*}p < 0.05$;$^{**}p < 0.01$).

reduction of LAMP2A presence when compared to CT (Fig. 5**B**). LAMP2A expression was especially located in neuronal somas and the proximal third of axons. In this region, few microglia expressed LAMP2A, so no analyses with IBA1 were performed. All statistical details in **Table S8**.

4. Discussion

Autophagy is involved in numerous molecular processes (Cao et al., 2021), making it a promising keystone for new therapeutic strategies (Condello et al., 2019). Here, we examined the autophagy pathway in the brain, studying its modulation in a stress-based model of depression. Autophagy has been characterized in a similar animal model (Shu et al., 2019; Wang et al., 2019; Xiao et al., 2018; Yang et al., 2017). However, no previous work had explored as deeply the impacts of chronic stress on autophagy in two brain structures, as well as its interplay with the ESCRT complex, which helps to clear autophagic cargo. Additionally, we traced the lysosomal profile changes due to the CMS protocol, which impair the main effectors of the CMA in FC and Hp.

Regarding the evaluation of macroautophagy markers, a distinct response to stress was observed in a region-specific manner, suggesting that autophagy either plays a particular role in each area or that their susceptibility to stress is specific. FC experienced protein downregulations in four of the chief mediators in the initiation and elongation processes. In basal conditions, mTOR maintains ULK1 inactive through phosphorylation, but when stress is present, mTOR is inhibited to promote the activation of ULK1 (Nazio and Cecconi, 2017). Although it is commonly stated that mTOR is suppressed by stress (Su and Dai, 2017), it is important to highlight that mTOR is a core protein in which many essential pathways converge, and it is part of two structural complexes, mTORC1 and mTORC2 (Su and Dai, 2017). It is not feasible to fathom the role that each system is playing with the present data. Likewise, contradictory literature describes how oxidative stress, which is increased in CMS (Martin-Hernandez et al., 2016), is able to both induce and suppress mTOR according to the intensity, duration, and nature of such stress (Su and Dai, 2017).

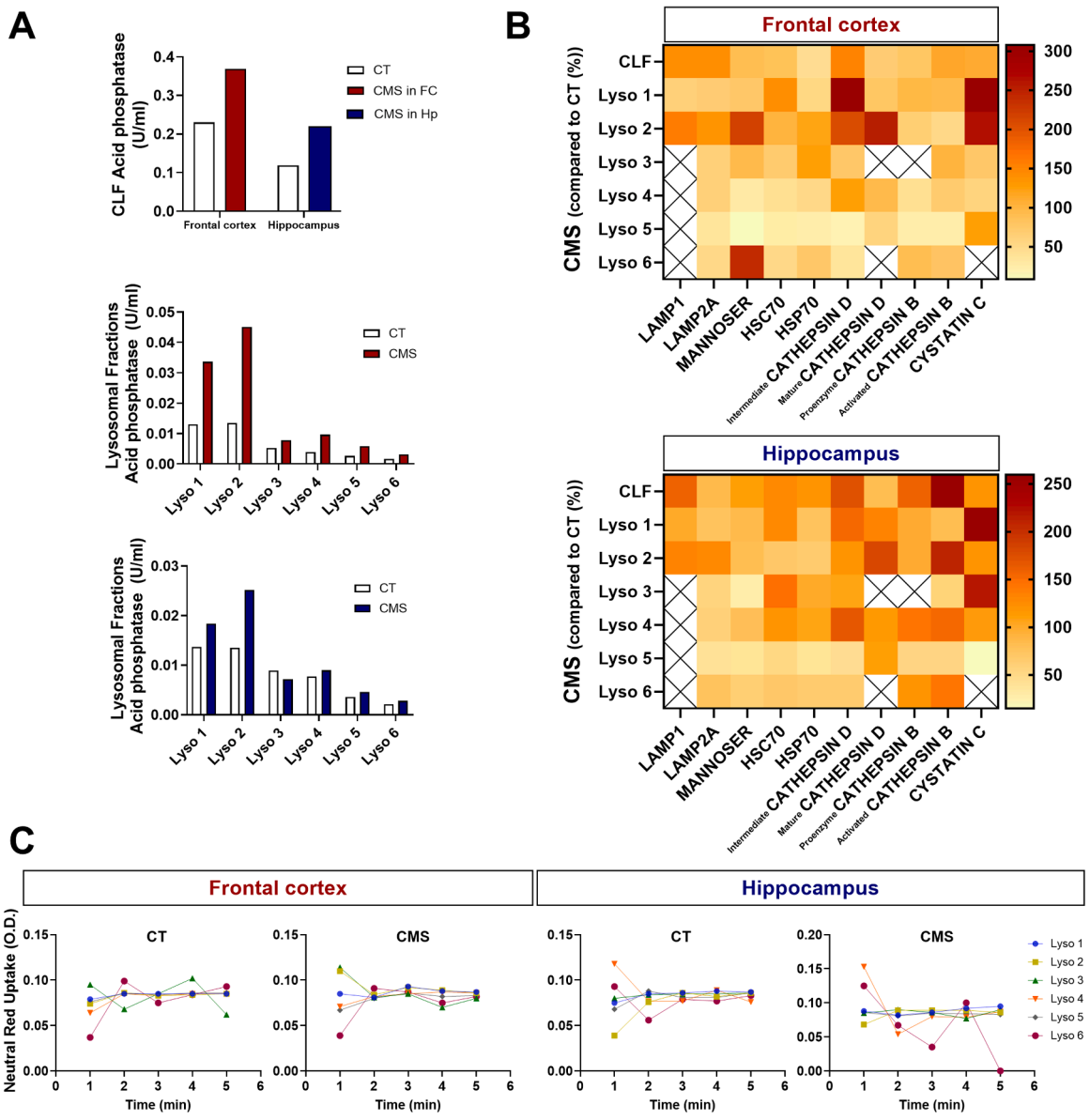

Fig. 4. CMS influence on the lysosome. Acid phosphatase enzyme levels were measured in crude lysosomal fractions (CLF) and in six purified fractions (Lyso 1 – Lyso 6), showing a general elevation in FC and Hp (**A**). WB analyses of chaperone-mediated autophagy (CMA) and lysosomal functional proteins represented in two color diagrams, showing distinct alterations according to lysosomal fraction and brain region (**B**). Neutral Red Uptake assay did not exhibit any difference in lysosomal integrity (**C**). Data is shown as the pool means of 6 CT and 6 CMS rats.

Hippocampal p-mTOR decreased, suggesting that each brain structure responds in an individually timely fashion. Upon cellular stress, mTOR phosphorylation is reduced to further diminish p-ULK1, facilitating ULK1 to bind with AMP-activated protein kinase (AMPK), activating BECLIN1 in turn and inducing lipidation of LC3I to LC3II (Hwang et al., 2017). Despite this, total protein values of BECLIN1 were lower in both areas, which might illustrate a hindrance in the nucleation step. SQSTM1/p62 acts as the cargo adaptor in the autophagy pathway, assembling with polyubiquitinated proteins and malfunctioning organelles, favoring their degradation through autophagy (Ro et al., 2014). The phosphorylation of SQSTM1/p62 is known to promote the autophagic degradation of SQSTM1/p62 and its products, enhancing its affinity for ubiquitinated chains and increasing their autophagic clearance (Matsumoto et al., 2011; Ro et al., 2014). ULK1 phosphorylates SQSTM1/p62, allowing autophagy to be set in motion by facilitating both SQSTM1/p62 and its cargo to reach the autophagosome site (Ro et al., 2014). Considering that CMS reduced ULK1 values in FC, it is possible that the phosphorylation was consequently impeded, leading to the accumulation of cargo waiting to be eliminated in the cytoplasm. ATG7 and ATG3 are E1/2-like and ubiquitin-like enzymes respectively, which are responsible for the addition of phosphatidylethanolamine (PE) to LC3I to form LC3II, and their oxidation may prevent the lipidation of LC3I to LC3II (Frudd et al., 2018). It is conceivable that the CMS-derived higher pro-oxidant environment (Martin-Hernandez et al., 2016), could alter ATG3 and ATG7 capabilities to interact with LC3, hampering the formation and maturation of autophagosomes, as evidenced by their protein levels. It might be possible that the stress-induced downregulation of ULK1 and BECLIN1 led to the increase of ATG7 at both protein and mRNA levels in FC. Since the ATG 16L1 complex is accountable for the double membrane elongation and the conjugation of PE to LC3 (Cao et al., 2021), the diminution in ATG 16L1 cortical values might hinder both processes, and aggravate the situation derived from the alterations in ATG3 and ATG7. Hippocampal ATG 16L1 increase could otherwise counteract the CMS-diminished ATG12 and

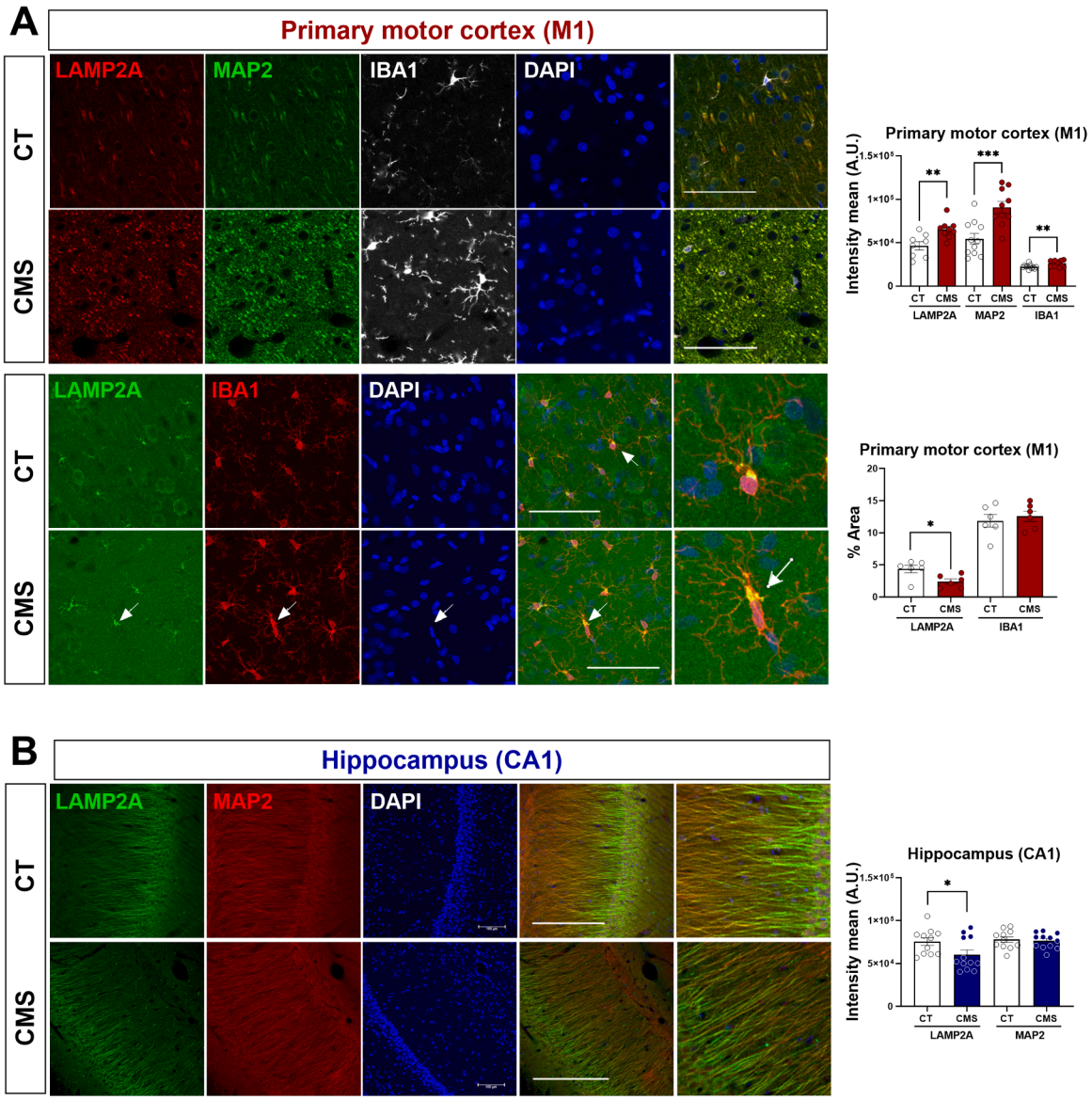

Fig. 5. CMS modifies LAMP2A expression in neurons (MAP2) and microglia (IBA1). Primary motor cortex (FC) displayed an elevation of the three markers attributable to CMS. The amount of area occupied by LAMP2A within the cortical microglia decreased in the CMS group, although more extended microglial somas and number of ramifications were visualized (**A**). Hippocampal CA1 neurons (MAP2+) were conversely subjected to a reduction of their LAMP2A protein content because of the CMS exposure (**B**). Analyses were made over the 20 X images, whose scale bars represent 200 μm. For 63 X images (microglia only), scale bars stand for 30 μm. Two-tailed Student *t*-test or Mann-Whitney test were used in the analysis of each marker. Data is expressed as mean ± SEM of 6–8 CT and CMS rats. (*$p < 0.05$;**$p < 0.01$).

ATG3; consequently, these downregulations could have induced their gene expression while additional ATG5 and ATG7 were needed to compensate for the modulations in the other autophagy-related markers. In this way, CMS altered autophagy initiation, nucleation, and elongation processes.

To evaluate the autophagic flux, leupeptin was injected intracortically and intrahippocampally, but no conclusive results were obtained as total inhibition was not achieved. This might be due to the latency period between the injection and sample collection, the metabolic rate at which brain cells eliminated the leupeptin, or an inadequate concentration.

Immunofluorescence data strongly suggest that SQSTM1/p62 phosphorylation occurs exclusively in astrocytes. To our knowledge, this is the first time that this specific connection has been made. Curiously, the immunostaining was not equal throughout the entire population of astrocytes, potentially indicating that specific astrocyte subpopulations undergo specific p-SQSTM1 modulation. Furthermore, p-SQSTM1 staining appears more intense in the soma-proximal regions. Overall, astrocytes react to cellular stress to protect neurons: impaired autophagy within these cells would directly affect neuronal homeostasis, resulting in neuronal damage, neurotransmission alterations, and impaired neuronal plasticity (Menard et al., 2017; Linnerbauer et al., 2020; Ortiz-Rodriguez and Arevalo, 2020). The CMS-promoted change of localization pattern in hippocampal CA3 cells, which was soma-oriented in CT groups but spread throughout astrocytic ramifications after CMS exposure, might indicate a precise function of Ser403 phosphorylation in astrocytes during the stress response.

The ESCRT complex consists of a membrane remodeling machinery crucial for membrane dynamics processes (Gatta and Carlton, 2019), comprising three subcomplexes: ESCRT-I, ESCRT-II, and ESCRT-III, along with another referred to as ESCRT-0, which allows the recruitment of the ESCRT subcomplexes themselves (Vietri et al., 2020). The

ESCRT machinery is involved in essential functions, such as autophagy, lysosomal and plasma membrane repair, and neuronal pruning (Remec Pavlin and Hurley, 2020; Vietri et al., 2020). Proxy proteins of each subcomplex were evaluated to understand their role in the stress response. Cortical HRS and STAM2 dysregulation could hamper the targeting and recruitment of downstream ESCRT products. This could explain the CMS-derived downregulation of TSG101, VPS28, and VPS37A in FC. ESCRT-I and II oversee the assembly of multiple factors needed for repair processes and membrane budding, eventually recruiting the ESCRT-III subcomplex. CMS increased ESCRT-III CHMP6, which participates in the polymerization step allowing membrane constriction and scission, which might be a compensatory cellular mechanism upon ESCRT-I dysregulation. Consequently, three key ESCRT functions could potentially be altered by CMS: protein sorting (Vietri et al., 2020), autophagosome formation (Gatta and Carlton, 2019; Vietri et al., 2020), and lysosome repair (Remec Pavlin and Hurley, 2020; Skowyra et al., 2018). Lysophagy follows ESCRT-mediated lysosomal repair, and it is initiated by galectins, such as GALECTIN3 (Radulovic et al., 2018). The multiple alterations in the cortical ESCRT machinery could lead to greater lysosomal damage, favoring the induction of GALECTIN3 for repair. Again, sensitivity to stress is region-specific. GALECTIN9 is required for efficient polyubiquitination during lysosomal damage (Jia et al., 2020), connecting membrane damage signals to the ubiquitin system and the ESCRT complex. Reduced GALECTIN9 protein concentrations lead to lower basal signaling, which would negatively impact ESCRT complex recruitment and polyubiquitination of the cargo to be degraded.

Considering the evidence pointing towards lysosomal damage, we checked whether CMS alone could influence the quantity of lysosomes. CMS increased acid phosphatase levels (used to test lysosomal preparation purity (Zhang et al., 2011)) in FC and Hp, possibly as a consequence of the accumulated cargo that was not adequately disposed of. Lysosomal fractions contained distinct lysosomes in nature: those at the top were light lysosomes, and those from the lower layers were heavy lysosomes (Schmidt et al., 2009). FC displayed a major increase in the first two purified fractions, exhibiting a higher susceptibility of light lysosomes to CMS. CMS might have generated lysosomal damage while it stimulated their biogenesis to better respond to stress, but as the autophagy was defective, there was not an appropriate lysosomal turnover. Next, some proteins related to the CMA and lysosomal function were assessed. LAMP2A, a core transporter in the CMA, was downregulated in light and heavy lysosomal fractions in both brain areas. During CMA, selected proteins are recognized by HSC70, which carries them towards LAMP2A and finally they are translocated into the lysosome lumen (Bonam et al., 2019; Kaushik and Cuervo, 2018). Changes observed in LAMP2A and HSC70 provide evidence of the lysosome stress response and the involvement of the CMA, which needs to be further evaluated. LAMP2A upregulation could be due to an increased transcription and to a stress-derived modified degradation rate (Kaushik and Cuervo, 2018). In CLF, FC and Hp showed opposite CMS-mediated regulation, illustrating that stress also modulates CMA in a particular fashion. Mannose-6-phosphate is conjugated into prospective lysosomal enzymes (Coutinho et al., 2012). Mannose receptor ensures that mannose-6-phosphate-binded residues are internalized into lysosomes for them to acquire their final phenotype. The CMS-mediated homogenic diminution of the receptor along hippocampal fractions evidenced that stress directly influenced it regardless of lysosomal nature. Many hydrolytic enzymes are sequestered within lysosomes (e.g., phosphatases and proteases). Cathepsins are the most prominent family of proteases (Kaminskyy and Zhivotovsky, 2012). Aspartic cathepsin D and cysteine cathepsin B exert a determining role in autophagy, both being enclosed into the lysosome through mannose-6-phosphate trafficking (Ishidoh and Kominami, 2002). The mature CATHEPSIN D reduction and the upregulation of activated CATHEPSIN B in CLF of each area concur with a study where a compensatory elevation of CATHEPSIN B levels and activity in neurons of CATHEPSIN D-deficient mice were observed (Koike et al., 2000). Mature CATHEPSIN D digests waste products and peptides, and it is also found in autolysosomes (Di et al., 2021). A diminished mature form contributes to the elevation of internal waste products within the lysosome. CYSTATIN C prevents cathepsins from being released into the cytoplasm and harm the cell (Amin et al., 2020). CYSTATIN C protein levels increased in lighter lysosomal fractions in both regions. Thus, the higher proteolytic environment (CYSTATIN C upregulation coincides with CATHEPSIN D elevation in fractions of FC and Hp) might surpass the basal inhibitory effects of cystatin proteases. Therefore, an elevated CYSTATIN C could be the cellular counterresponse to the increment of cathepsins, which could have been previously upregulated in an attempt to eliminate the accumulated cargo caused by an impaired autophagy. Interestingly, CYSTATIN C protein levels are higher in sera of patients suffering from severe depression (Amin et al., 2020). All these results combined highlight the role of the lysosome in the stress response and brain homeostasis.

LAMP2A augmentation in the primary motor cortex aligned with WB results, taking place in neuronal and microglial lysosomes according to our immunofluorescence studies. CMS contributed to the increase of MAP2, which attaches to microtubules and modulates their stability (Marchisella et al., 2016). Upregulated MAP2 protein levels might lead to a higher microtubule polymerization, causing a disbalance in dendrite arborizations and neuronal stability. Lysosomes are usually disposed in the perinuclear site and in the cell periphery (Cabukusta and Neefjes, 2018). MAP2 selectively upholds lysosomes around the neuronal soma, while distributing cargos along neurons (Gumy et al., 2017): no changes in hippocampal MAP2 were associated with their unmodified perinuclear location. In FC, MAP2 upregulation in CMS could have obstructed basal microtubule function, and hence, its control over lysosomal distribution. Although soma enlargement and more ramifications were observed in cortical microglia, CMS contributed to lysosomal concentration, presumably to better respond to stress.

Although this study provides important insights into the role of autophagy and the ESCRT complex after exposure to CMS, some limitations should be noted. First, the use of a rodent model may not fully summarize the complexity of human MDD, limiting the translatability of the findings. Second, this study lacks pharmacological validation, as no direct inhibitors or activators of autophagy pathways were utilized to confirm the causal relationships between the observed changes and the CMS. Addressing these limitations in future studies would be necessary to augment the strength and applicability of our findings.

In summary, our data point to a CMS-induced accumulation of misfolded proteins and aggregates due to an altered autophagy and disrupted lysosomal homeostasis, together with the potential intensification of polyubiquitinated proteins derived from the ESCRT complex alterations. This work provides several shreds of evidence about the distinct modulation that stress exerts in FC and Hp, highlighting the importance of further scrutinizing autophagy and its playmates according to organs and specific locations. Furthermore, a potential new function has been described related to glial autophagy: Ser403 phosphorylation of SQSTM1/p62 only happens within astrocytes, and stress changes their local distribution towards their ramifications. Further research is warranted to unravel this implication and its possible exploitation to develop additional therapeutic strategies. Comprehending the part that autophagy plays in each brain region would aid in understanding how its pharmacological modulation could be exploited to improve the current stress-related and neuropsychiatric disorders treatments.

Declaration of generative AI and AI-assisted technologies in the writing process

During the preparation of this work the authors used ChatGPT in order to correct and refine the English. After using this tool/service, the authors reviewed and edited the content as needed and take full

responsibility for the content of the publication.

Funding

Funding for this study was provided by Spain's Ministry of Science, Innovation and Universities (MICIU), the *Agencia Estatal de Investigación* (AEI; 10.13039/501100011033) and the European Regional Development Fund (FEDER) (PID2020–113103RB-I00, PID2020–118189RB-I00, and PID2023–146894NB-I00) and CIBERSAM-ISCIII (CB/07/09/0026). CUM was a FPU fellowship from the Spain's Ministry of Universities. The MICIU, AEI, FEDER and CIBERSAM-ISCIII had no further role in study design; in the collection, analysis and interpretation of data; in the writing of the report; and in the decision to submit the paper for publication.

CRediT authorship contribution statement

Cristina Ulecia-Morón: Investigation, Formal analysis, Conceptualization, Writing – original draft. **Álvaro G. Bris:** Investigation, Validation. **Karina S. MacDowell:** Investigation, Validation. **Pilar Cerveró-García:** Investigation, Validation. **José L.M. Madrigal:** Formal analysis, Writing – review & editing. **Borja García-Bueno:** Formal analysis, Writing – review & editing. **Marta P. Pereira:** Investigation, Validation. **Juan C. Leza:** Formal analysis, Writing – review & editing. **Javier R. Caso:** Conceptualization, Funding acquisition, Supervision, Writing – review & editing.

Declaration of competing interest

All authors declare that they have no conflicts of interest.

Acknowledgments

We thank the Animal Facility as well as the enter for Microscopy and Flow Cytometry of the Complutense University of Madrid. We are also thankful to Ms. Beatriz Moreno for helping with the extraction protocols.

Supplementary materials

Supplementary material associated with this article can be found, in the online version, at doi:10.1016/j.euroneuro.2025.02.005.

References

Amin, F., Khan, M.S., Bano, B., 2020. Mammalian cystatin and protagonists in brain diseases. J. Biomol. Struct. Dyn. 38, 2171–2196.
Arango, C., Dragioti, E., Solmi, M., Cortese, S., Domschke, K., Murray, R.M., Jones, P.B., Uher, R., Carvalho, A.F., Reichenberg, A., et al., 2021. Risk and protective factors for mental disorders beyond genetics: an evidence-based atlas. World Psychiatry 20, 417–436.
Beurel, E., Toups, M., Nemeroff, C.B., 2020. The bidirectional relationship of depression and inflammation: double trouble. Neuron 107, 234–256.
Bhatt, S., Nagappa, A.N., Patil, C.R., 2020. Role of oxidative stress in depression. Drug Discov. Today 25, 1270–1276.
Bonam, S.R., Wang, F., Muller, S., 2019. Lysosomes as a therapeutic target. Nat. Rev. Drug Discov. 18, 923–948.
Bravo, L., Mico, J.A., Rey-Brea, R., Perez-Nievas, B., Leza, J.C., Berrocoso, E., 2012. Depressive-like states heighten the aversion to painful stimuli in a rat model of comorbid chronic pain and depression. Anesthesiology 117, 613–625.
Cabukusta, B., Neefjes, J., 2018. Mechanisms of lysosomal positioning and movement. Traffic 19, 761–769.
Cao, W., Li, J., Yang, K., Cao, D., 2021. An overview of autophagy: mechanism, regulation and research progress. Bull. Cancer 108, 304–322.
Collaborators GBDMD, 2022. Global, regional, and national burden of 12 mental disorders in 204 countries and territories, 1990-2019: a systematic analysis for the Global Burden of Disease Study 2019. Lancet Psychiatry 9, 137–150.
Condello, M., Pellegrini, E., Caraglia, M., Meschini, S., 2019. Targeting autophagy to overcome human diseases. Int. J. Mol. Sci. 20, 725.
Coutinho, M.F., Prata, M.J., Alves, S., 2012. A shortcut to the lysosome: the mannose-6-phosphate-independent pathway. Mol. Genet. Metab. 107, 257–266.
Deretic, V., 2021. Autophagy in inflammation, infection, and immunometabolism. Immunity 54, 437–453.
Di, Y.Q., Han, X.L., Kang, X.L., Wang, D., Chen, C.H., Wang, J.X., Zhao, X.F., 2021. Autophagy triggers CTSD (cathepsin D) maturation and localization inside cells to promote apoptosis. Autophagy 17, 1170–1192.
Frudd, K., Burgoyne, T., Burgoyne, J.R., 2018. Oxidation of Atg3 and Atg7 mediates inhibition of autophagy. Nat. Commun. 9, 95.
Gassen, N.C., Hartmann, J., Zschocke, J., Stepan, J., Hafner, K., Zellner, A., Kirmeier, T., Kollmannsberger, L., Wagner, K.V., Dedic, N., et al., 2014. Association of FKBP51 with priming of autophagy pathways and mediation of antidepressant treatment response: evidence in cells, mice, and humans. PLoS Med. 11, e1001755.
Gassen, N.C., Rein, T., 2019. Is there a role of autophagy in depression and antidepressant action? Front. Psychiatry 10, 337.
Gatta, A.T., Carlton, J.G., 2019. The ESCRT-machinery: closing holes and expanding roles. Curr. Opin. Cell Biol. 59, 121–132.
Gulbins, A., Schumacher, F., Becker, K.A., Wilker, B., Soddemann, M., Boldrin, F., Muller, C.P., Edwards, M.J., Goodman, M., Caldwell, C.C., et al., 2018. Antidepressants act by inducing autophagy controlled by sphingomyelin-ceramide. Mol. Psychiatry 23, 2324–2346.
Gumy, L.F., Katrukha, E.A., Grigoriev, I., Jaarsma, D., Kapitein, L.C., Akhmanova, A., Hoogenraad, C.C., 2017. MAP2 defines a pre-axonal filtering zone to regulate KIF1-versus KIF5-dependent cargo transport in sensory neurons. Neuron 94, 347–362 e347.
Habib, E., Cook, A., Mathavarajah, S., Dellaire, G., 2021. Adding some "splice" to stress eating: autophagy, ESCRT and alternative splicing orchestrate the cellular stress response. Genes (Basel) 12, 1196.
Hwang, J.Y., Gertner, M., Pontarelli, F., Court-Vazquez, B., Bennett, M.V., Ofengeim, D., Zukin, R.S., 2017. Global ischemia induces lysosomal-mediated degradation of mTOR and activation of autophagy in hippocampal neurons destined to die. Cell Death. Differ. 24, 317–329.
Ishidoh, K., Kominami, E., 2002. Processing and activation of lysosomal proteinases. Biol. Chem. 383, 1827–1831.
Jernigan, C.S., Goswami, D.B., Austin, M.C., Iyo, A.H., Chandran, A., Stockmeier, C.A., Karolewicz, B., 2011. The mTOR signaling pathway in the prefrontal cortex is compromised in major depressive disorder. Prog. Neuropsychopharmacol. Biol. Psychiatry 35, 1774–1779.
Jia, J., Bissa, B., Brecht, L., Allers, L., Choi, S.W., Gu, Y., Zbinden, M., Burge, M.R., Timmins, G., Hallows, K., et al., 2020. AMPK, a regulator of metabolism and autophagy, is activated by lysosomal damage via a novel galectin-directed ubiquitin signal transduction system. Mol. Cell 77, 951–969.
Jia, J., Le, W., 2015. Molecular network of neuronal autophagy in the pathophysiology and treatment of depression. Neurosci. Bull. 31, 427–434.
Kaminskyy, V., Zhivotovsky, B., 2012. Proteases in autophagy. Biochim. Biophys. Acta 1824, 44–50.
Kaushik, S., Cuervo, A.M., 2018. The coming of age of chaperone-mediated autophagy. Nat. Rev. Mol. Cell Biol. 19, 365–381.
Koike, M., Nakanishi, H., Saftig, P., Ezaki, J., Isahara, K., Ohsawa, Y., Schulz-Schaeffer, W., Watanabe, T., Waguri, S., Kametaka, S., et al., 2000. Cathepsin D deficiency induces lysosomal storage with ceroid lipofuscin in mouse CNS neurons. J. Neurosci. 20, 6898–6906.
Linnerbauer, M., Wheeler, M.A., Quintana, F.J., 2020. Astrocyte crosstalk in CNS inflammation. Neuron 108, 608–622.
Madrigal, J.L., Moro, M.A., Lizasoain, I., Lorenzo, P., Leza, J.C., 2002. Stress-induced increase in extracellular sucrose space in rats is mediated by nitric oxide. Brain Res. 938, 87–91.
Madrigal, J.L., Olivenza, R., Moro, M.A., Lizasoain, I., Lorenzo, P., Rodrigo, J., Leza, J.C., 2001. Glutathione depletion, lipid peroxidation and mitochondrial dysfunction are induced by chronic stress in rat brain. Neuropsychopharmacology 24, 420–429.
Marchisella, F., Coffey, E.T., Hollos, P., 2016. Microtubule and microtubule associated protein anomalies in psychiatric disease. Cytoskeleton (Hoboken) 73, 596–611.
Martin-Hernandez, D., Bris, A.G., MacDowell, K.S., Garcia-Bueno, B., Madrigal, J.L., Leza, J.C., Caso, J.R., 2016. Modulation of the antioxidant nuclear factor (erythroid 2-derived)-like 2 pathway by antidepressants in rats. Neuropharmacology 103, 79–91.
Matsumoto, G., Wada, K., Okuno, M., Kurosawa, M., Nukina, N., 2011. Serine 403 phosphorylation of p62/SQSTM1 regulates selective autophagic clearance of ubiquitinated proteins. Mol. Cell 44, 279–289.
Menard, C., Pfau, M.L., Hodes, G.E., Kana, V., Wang, V.X., Bouchard, S., Takahashi, A., Flanigan, M.E., Aleyasin, H., LeClair, K.B., et al., 2017. Social stress induces neurovascular pathology promoting depression. Nat. Neurosci. 20, 1752–1760.
Nazio, F., Cecconi, F., 2017. Autophagy up and down by outsmarting the incredible ULK. Autophagy 13, 967–968.
Nestler, E.J., Barrot, M., DiLeone, R.J., Eisch, A.J., Gold, S.J., Monteggia, L.M., 2002. Neurobiology of depression. Neuron 34, 13–25.
Ortiz-Rodriguez, A., Arevalo, M.A., 2020. The contribution of astrocyte autophagy to systemic metabolism. Int. J. Mol. Sci. 21, 2479.
Pandey, G.N., Rizavi, H.S., Bhaumik, R., Ren, X., 2019. Innate immunity in the postmortem brain of depressed and suicide subjects: role of toll-like receptors. Brain Behav. Immun. 75, 101–111.
Radulovic, M., Schink, K.O., Wenzel, E.M., Nahse, V., Bongiovanni, A., Lafont, F., Stenmark, H., 2018. ESCRT-mediated lysosome repair precedes lysophagy and promotes cell survival. EMBO J. 37, e99753.
Remec Pavlin, M., Hurley, J.H., 2020. The ESCRTs - converging on mechanism. J. Cell Sci. 133, jcs240333.
Ro, S.H., Semple, I.A., Park, H., Park, H., Park, H.W., Kim, M., Kim, J.S., Lee, J.H., 2014. Sestrin2 promotes unc-51-like kinase 1 mediated phosphorylation of p62/sequestosome-1. FEBS J. 281, 3816–3827.

Schmidt, H., Gelhaus, C., Lucius, R., Nebendahl, M., Leippe, M., Janssen, O., 2009. Enrichment and analysis of secretory lysosomes from lymphocyte populations. BMC Immunol. 10, 41.
Schreiber, E., Matthias, P., Muller, M.M., Schaffner, W., 1989. Rapid detection of octamer binding proteins with 'mini-extracts', prepared from a small number of cells. Nucleic. Acids. Res. 17, 6419.
Shu, X., Sun, Y., Sun, X., Zhou, Y., Bian, Y., Shu, Z., Ding, J., Lu, M., Hu, G., 2019. The effect of fluoxetine on astrocyte autophagy flux and injured mitochondria clearance in a mouse model of depression. Cell Death. Dis. 10, 577.
Skowyra, M.L., Schlesinger, P.H., Naismith, T.V., Hanson, P.I., 2018. Triggered recruitment of ESCRT machinery promotes endolysosomal repair. Science 360, eaar5078.
Su, K.H., Dai, C., 2017. mTORC1 senses stresses: coupling stress to proteostasis. Bioessays 39, 1600268.
Tomoda, T., Yang, K., Sawa, A., 2020. Neuronal autophagy in synaptic functions and psychiatric disorders. Biol. Psychiatry 87, 787–796.
Troubat, R., Barone, P., Leman, S., Desmidt, T., Cressant, A., Atanasova, B., Brizard, B., El Hage, W., Surget, A., Belzung, C., et al., 2021. Neuroinflammation and depression: a review. Eur. J. Neurosci. 53, 151–171.
Untergasser, A., Cutcutache, I., Koressaar, T., Ye, J., Faircloth, B.C., Remm, M., Rozen, S. G., 2012. Primer3–new capabilities and interfaces. Nucleic. Acids Res. 40, e115.
Vietri, M., Radulovic, M., Stenmark, H., 2020. The many functions of ESCRTs. Nat. Rev. Mol. Cell Biol. 21, 25–42.
Wang, M., Bi, Y., Zeng, S., Liu, Y., Shao, M., Liu, K., Deng, Y., Wen, G., Sun, X., Zeng, P., et al., 2019. Modified Xiaoyao San ameliorates depressive-like behaviors by triggering autophagosome formation to alleviate neuronal apoptosis. Biomed. PharmacOther 111, 1057–1065.
Willner, P., 2005. Chronic mild stress (CMS) revisited: consistency and behavioural-neurobiological concordance in the effects of CMS. Neuropsychobiology 52, 90–110.
Xiao, X., Shang, X., Zhai, B., Zhang, H., Zhang, T., 2018. Nicotine alleviates chronic stress-induced anxiety and depressive-like behavior and hippocampal neuropathology via regulating autophagy signaling. Neurochem. Int. 114, 58–70.
Yang, L., Zhao, Y., Wang, Y., Liu, L., Zhang, X., Li, B., Cui, R., 2015. The effects of psychological stress on depression. Curr. Neuropharmacol. 13, 494–504.
Yang, Y., Hu, Z., Du, X., Davies, H., Huo, X., Fang, M., 2017. miR-16 and fluoxetine both reverse autophagic and apoptotic change in chronic unpredictable mild stress model rats. Front. Neurosci. 11, 428.
Zhang, F., Xu, M., Han, W.Q., Li, P.L., 2011. Reconstitution of lysosomal NAADP-TRP-ML1 signaling pathway and its function in TRP-ML1(-/-) cells. Am. J. Physiol. Cell Physiol. 301, C421–C430.